RESEARCH ARTICLE

Effect of Sulfurization Temperature on RF Sputtered MoS_2 Thin Film

V. Thiruvengadam[1], Braj Bhusan Singh[1], Palash Kumar Manna[1], Subhankar Bedanta[1,2,*]

[1]Laboratory for Nanomagnetism and Magnetic Materials (LNMM), School of Physical Sciences, National Institute of Science Education and Research (NISER), HBNI, P.O. Bhimpur Padanpur, Via Jatni, 752050, India
[2]Center for Interdisciplinary Sciences (CIS), National Institute of Science Education and Research (NISER), HBNI, P.O. Bhimpur Padanpur, Via Jatni, 752050, India

***Corresponding author: E-mail: sbedanta@niser.ac.in**

DOI: 10.5185/amlett.2021.021603

Molybdenum disulfide (MoS_2) is one among the transition-metal dichalcogenide (TMD) family which exhibits exotic physical properties at their mono-layer limit. We report a facile way to fabricate stoichiometric, crystalline and star shaped MoS_2 film. In this work, ultra-thin MoS_2 films were fabricated by two step process (i) RF sputtering of MoS_2 target followed by (ii) sulfurization to improve stoichiometry and crystallinity. In order to study the effect of sulfurization temperature on sputtered MoS_2, sulfurization has been performed at five different temperatures - 700, 750, 775, 800 and 825°C. Surface morphology of as sputtered and sulfurized MoS_2 films were characterized using optical and scanning electron microscopes. Crystallinity and layer thickness of the fabricated MoS_2 films were estimated by using Laser Raman spectroscopy. These results confirm that as sputtered MoS_2 films are discontinuous, amorphous in nature and it crystalizes into a layered structure during sulfurization at temperature ≥ 750°C. It was observed that at sulfurization temperature of 800°C, the nucleated crystallites well grown into a star shaped crystalline MoS_2 with their thickness vary between 2 and 3 mono-layers. These star shapes can provide more surface area/edges that can be exploited to enhance the efficiency of gas sensors.

Introduction

Two dimensional transition metal dichalcogenides (TMDs) are some of the most researched materials for next generation ultra-thin electronic devices, optoelectronic devices and valleytronic physics [**1,2**]. Molybdenum disulfide (MoS_2) is one among the TMD family composed of an atomic layer of Molybdenum sandwiched covalently between two layers of sulfur atoms (S-Mo-S) in a trigonal prismatic geometry [**3-5**]. MoS_2 at its monolayer limit exhibits a transition from indirect band gap (1.23 eV) to direct band gap (1.88 eV) that leads to a strong photo luminescence [**6**]. At the monolayer limit it also shows confinement of electrons and holes vertically along the layer thickness [**7,8**] and valley polarization of electrons [**4**]. These properties make them interesting candidate not only for the electronic and optoelectronic applications but also for fundamental physics such as valleytronics, where the valley degree of electron has been accessed for application. Apart from these, MoS_2 has also been used for sensing applications. The mechanism behind the sensing property of MoS_2 is the change of its electrical properties due to charge transfer between adsorbed analyte molecules and MoS_2 [**9-12**]. DFT calculations show that the surface of MoS_2 has strong interaction with the pollutant gasses such as NO_2, NO and SO_2 [**13,14**]. The sensing capability of MoS_2 has experimentally been demonstrated for various analytes such as NO, CO, NO_2, NH_3, H_2S, triethylamine, xylene and methanol [**15-18**]. Adsorption of the gas molecules on solid surfaces happens mostly on the steps, edges, terraces, kinks and corner atoms of a substance where the atomic coordination is low [**19**]. Therefore, the sensitivity of the MoS_2 based sensors can be improved by fabricating different morphologies (e.g. triangles, stars) of MoS_2. Various top-down as well as bottom-up approaches have been reported for fabricating mono to few-layer MoS_2. They are mechanical, electrochemical and liquid phase exfoliation [**20-22**], solution sonication [**23**], laser and plasma thinning [**24,25**], chemical vapour [**26,27**], physical vapour [**28-30**] and atomic layer deposition [**31,32**] techniques. Of the above mentioned various fabrication techniques, only CVD and ALD techniques fabricate atomically thin MoS_2 with triangular and star shapes that are essential for gas sensing application. However, these techniques are not scalable as sputtering technique. On the other hand, sputtering technique demonstrates continuous film of amorphous and non-stoichiometric MoS_2 with sulfur vacancies [**33**]. This could be due to the difference in sputtering yield and vapour pressure of Mo and S atoms. However, C. Muratore *et. al.,* fabricated a few-layer crystalline MoS_2 by direct sputtering of MoS_2 target [**28**]. In order to complement the sulfur vacancies as well us to improve the crystallinity of as sputtered film, sulfurization or/and annealing was performed at elevated temperature based on the sputter target (Mo or MoS_2) used [**1,28,34**]. W. Zhong *et. al.,* and J. Haung *et. al.,* reported large-area few-layer MoS_2 by RF sputtering of MoS_2 target followed by sulfurization process [**35,36**]. H. Samassekou *et. al.,* and

S. Hussain *et. al.*, showed 4-layer and 2 to a few-layer of MoS_2 by RF magnetron sputtering of MoS_2 target followed by a post deposition annealing treatment [**37,38]**. S. Hussain *et. al.*, fabricated bi-layer to tri-layer of MoS_2 by reactive sputter deposition of MoO_3 ultra-thin film followed by conversion of MoO_3 film to MoS_2 by sulfurization [**38**]. R. Gatensby *et. al.*, R. Shahzad *et. al.*, and N. Choudhary *et. al.*, fabricated mono to multi – layer MoS_2 by depositing different thickness of Mo by sputtering of Mo target followed by sulfurization process [**1,34,39]**. Advantage of the sputtering over other techniques is cleanliness of the fabricated films and nanostructures due to ultra-high vacuum (UHV) processing condition of the technique [**28**].

Sputtering technique for the fabrication of mono- to few- layer MoS_2 follows two methods in general; (i) sputter deposition of Mo thin film followed by converting it into crystalline MoS_2 by sulfurization process [**1,33,39-42**] , (ii) sputter deposition of amorphous MoS_2 thin film (with S deficiency) followed by sulfurization process to convert amorphous MoS_2 into crystalline MoS_2 [**35,36,43,44]**. From this, it is clear that the sulfurization is an essential process independent of depositing Mo or MoS_2 for fabricating crystalline MoS_2 film using sputtering technique. So far, the effect of sputtering time and substrate temperature during deposition have been well studied. However, there is not much of studies focused on effect of sulfurization temperature on sputtered Mo or MoS_2 films. In addition fabrication of different morphologies of MoS_2 which are essential for gas sensing application has not been demonstrated using sputtering technique.

In this work we have attempted to fabricate atomically thin star shaped MoS_2 film by RF magnetron sputtering of commercially available stoichiometric MoS_2 target followed by sulfurization process. In order to conduct a systematic study on effect of sulfurization temperature on sputtered MoS_2 films, we have performed the sulfurization at different temperatures. The resulting MoS_2 films were characterized for their morphology, crystalline quality and layer thickness by using optical microscope, scanning electron microscope and laser Raman spectroscopy.

Experimental

Crystalline MoS_2 films were fabricated by two steps; (i) RF magnetron sputtering of MoS_2 films followed by (ii) sulfurization of as deposited films, a process of annealing in an environment of sulfur vapour. MoS_2 thin film of thickness 0.7 nm was fabricated on B doped P-type Si (100) substrate by RF magnetron sputtering of commercially available stoichiometric MoS_2 target. Prior to deposition, the Si substrate was ultrasonically cleaned with acetone and ethanol followed by dried with N_2 gas. For MoS_2 thin film deposition, as cleaned Si substrate was loaded in to high vacuum multi-deposition system (Make: Mantis Deposition Ltd., UK) with a base pressure of 1.24×10^{-7} mbar. MoS_2 target was sputtered by applying RF input power of 46 Watt. The deposition was carried out for 70 s at a deposition pressure of 5.5×10^{-3} mbar with Ar flow and deposition rate of 15 SCCM and 0.1 Å/s respectively.

For sulfurization process, as sputtered MoS_2 film was transferred into a single zone quartz tube furnace. Sulfurization was performed at five different temperatures - 700, 750, 775, 800 and 850°C for 4 hours in N_2 atmosphere with N_2 flow rate of 100 SCCM and the tube pressure was maintained between 3.75 to 3.85 Torr. During sulfurization process, the sputtered MoS_2 thin film was kept on central zone of the tube furnace whereas the alumina boat containing sulfur powder (99.98% of purity from Sigma-Aldrich) was kept on upstream of the tube furnace. The place for the alumina boat in the tube furnace was chosen in such a way that the temperature of the sulfur powder always reaches above 120°C (above the melting point of sulfur ~ 115°C). The distance between the boat containing sulfur powder and the sputtered thin film was kept same for all sulfurization temperatures. The as sputtered MoS_2 thin film and the films sulfurized at 700, 750, 775, 800 and 850°C were designated as S0, S1, S2, S3, S4 and S5, respectively. Surface morphology of as-sputtered as well as the sulfurized MoS_2 films were characterized using both optical and scanning electron microscope (SEM). The crystallinity and layer thickness of the MoS_2 films were characterized using laser Raman spectroscopy (Make: HORIBA LabRAM HR Evolution) with laser wavelength of 532 nm.

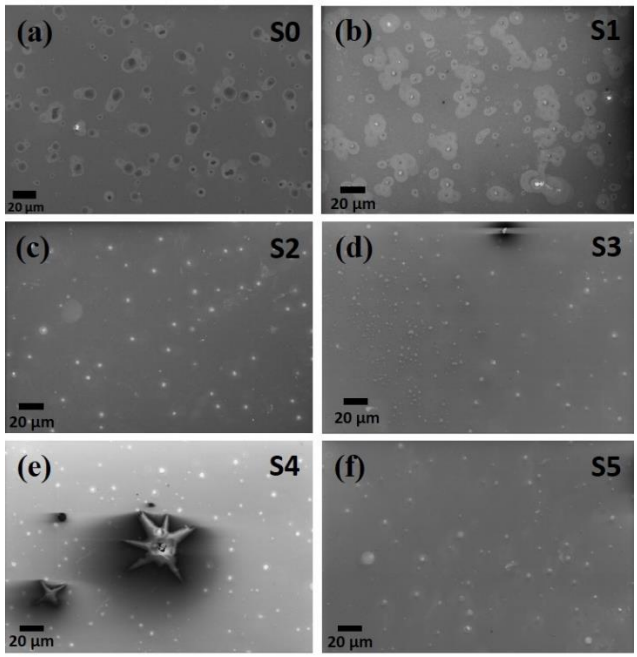

Fig. 1. Scanning electron micrographs of (a) as sputtered MoS_2 film, MoS_2 films sulfurized at (b) 700°C, (c) 750°C, (d) 775°C, (e) 800°C and (f) 850°C.

Results and discussion

Scanning electron micrographs of as deposited MoS_2 film as well as the films post-sulfurized at different temperatures are shown in **Fig. 1**. SEM image of as sputtered sample shows many circular spots with a dot structure at the centre of the circular spot. These island structures indicate that as deposited MoS_2 film is discontinuous. SEM images of all

the sulfurized samples shows number of dot patterns at random places of the sample. Apart from these dots, sample S4 shows star shaped islands of size ~ 40 to 100 µm in random places of the sample. Formation of star shape nano-island by the transition metal dichalcogenides has already been reported theoretically. The formation of the star shapes can be understood as follows. In the beginning of the sulfurization process, MoS_2 nucleates as circular dots with zigzag Mo, zigzag S and arm chair Mo-S edges. With increasing growth time, these dots turn into triangular shape due to difference in growth rates of zigzag S and zigzag Mo with the highest and lowest growth rates, respectively [**45**]. Theoretical results suggest that these triangular shaped MoS_2 islands can morph into star shapes because of two reasons: (i) merging of multiple triangular island growing concurrently, and (ii) formation of inversion-domains due to chalcogen deficiency [**46**].

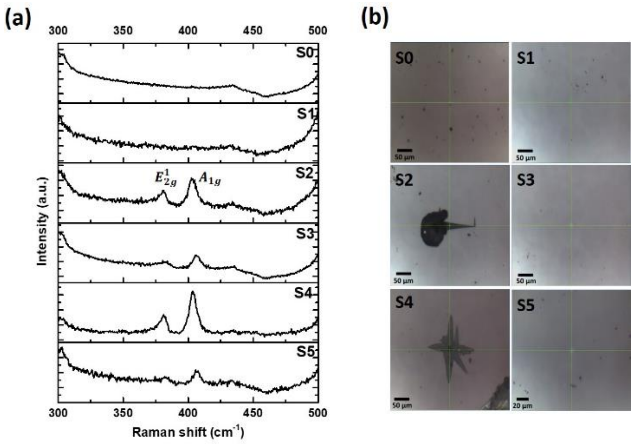

Fig. 2. Raman Spectra of (a) as sputtered and sulfurized MoS_2 film and (b) corresponding optical images.

In order to confirm the formation of crystalline MoS_2 and to estimate its layer thickness, as sputtered and sulfurized films were characterized using laser Raman spectroscopy [**3**]. **Fig. 2** shows the Raman spectra of as sputtered MoS_2 film as well as the films post-sulfurized at different temperatures along with their optical images (from where the Raman spectra were collected). The optical images of all the samples including the as sputtered one shows random irregular dot like island structures. Apart from those spots, the sample S4 shows star shaped island of size which varies between 40 to 100 µm in random places. These optical images are consistent with the images obtained from SEM. Raman spectra of as sputtered MoS_2 film and the sample sulfurized at 700°C does not exhibit characteristic peaks for MoS_2. Sample fabricated with sulfurization temperature of above 700°C and up to 800°C, exhibit E^1_{2g} (~382 cm^{-1}) and A_{1g} (~408 cm^{-1}) MoS_2 characteristic Raman peaks selectively at dot or star shaped islands that are shown in corresponding optical images. These Raman peaks were found to disappear while moving away from this island structures. This signifies that only those island structures are MoS_2 and the remaining are bare Si substrate.

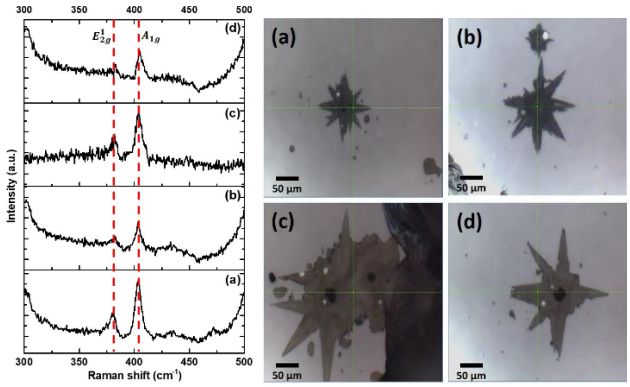

Fig. 3. Raman Spectra (a to d) from star-shaped MoS_2 that grown at different places of the sample S4 that sulfurized at 800°C and corresponding optical images.

The results from SEM images and Raman spectra together confirm that as sputtered MoS_2 films are discontinuous and amorphous in nature. These discontinuous and amorphous MoS_2 crystallize during the sulfurization process. Absence of Raman peaks for MoS_2 in the sample that sulfurized at 700°C indicates that those samples are still amorphous in nature. This implies that the 700°C of sulfurization temperature is insufficient for the crystallization of the sputtered amorphous MoS_2 island. Appearance of the Raman peaks for MoS_2 in the samples sulfurized at 725°C and above indicates proper crystallization of amorphous MoS_2 islands. Layer thickness of the crystallized MoS_2 in the sulfurized samples were estimated by calculating the frequency difference between E^1_{2g} and A_{1g} Raman modes [**3,39**]. The frequency difference between these two Raman modes were found to be 23.3 cm^{-1}, 24.6 cm^{-1}, 22.6 cm^{-1} and 24.7 cm^{-1} in sample S2, S3, S4 and S5 respectively. These numbers indicates that the MoS_2 layer thickness in S2, S3, S4 and S5 are of 3, 4, 2 and 4 mono-layers respectively [**3,39**]. Out of all the four samples, sample S4 which is sulfurized at 800°C, shows the thinnest MoS_2 film having two layers of MoS_2 with peculiar star-shaped island [**46,47**]. Also, Raman spectra have been performed on different star-shaped islands at various places of the sample S4 (**Fig. 3**) and different spots on the same star-shaped island (**Fig. 4**) to check the variation in MoS_2 layer thickness between the various islands and within the same island. Between various MoS_2 islands as well as with in the same island the layer thickness varies from 2 to 3 monolayer of MoS_2. To crosscheck the thickness of MoS_2 further, we have characterized the sample S4 using photoluminescence (PL) spectroscopy. The PL spectra of MoS_2 at its mono-layer thickness are known to exhibit a strong emission peak due to direct band gap - a distinctive property of mono-layer MoS_2 [**34,48**]. However, the PL spectra of sample S4 (not shown here) did not show any such emission peak. This result implies that the MoS_2 in sample S4 is not a mono-layer and it is consistent with the Raman spectroscopy results which show 2 to 3 monolayer thickness of MoS_2 in sample S4. All these results clearly indicate that as

sputtered MoS_2 is amorphous in nature and it nucleate in to layered crystallite structure for the sulfurization temperature of 750°C and above. At sulfurization temperature of 800°C, the nucleated crystallite well grown into a star shaped crystalline MoS_2 with their thickness vary between 2 and 3 monolayer.

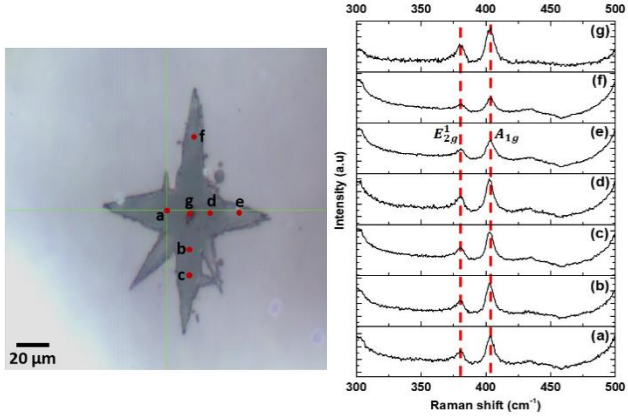

Fig. 4. Raman Spectra from different places of a star-shaped MoS_2 that grown at the sample S4.

Conclusion

In summary, star shaped ultra-thin MoS_2 films were fabricated by RF sputtering of MoS_2 target followed by sulfurization process. In order to check the effect of sulfurization process on the crystalline quality of the MoS_2 film, sulfurization was performed at different temperatures, 700, 750, 775, 800 and 825°C. All these MoS_2 films were characterized for their morphology, crystalline quality and layer thickness by optical microscope, scanning electron microscope and laser Raman spectrometer. Results from microscopy and Raman spectroscopy together conclude that as sputtered MoS_2 film is discontinuous and amorphous in nature. These discontinuous and amorphous MoS_2 crystallize into layered structure during the sulfurization at temperature $\geq$ 750°C. It has also been observed that at sulfurization temperature of 800°C, the nucleated crystallites well grown into a star shaped crystalline MoS_2 with their thickness vary between 2 and 3 monolayer. These star-shaped MoS_2 islands can have potential application in gas sensors due to larger surface area/edges.

Acknowledgements

We acknowledge the financial support from Department of Science and Technology (DST)-Nanomission (SR/NM/NS-1018/2016(G)), Government of India. We also thank Department of Atomic energy for the support for various research facilities. BBS thank DST-INSPIRE programme for the INSPIRE faculty fellowship.

Conflicts of interest

The authors declare that there is no conflict of interest.

Keywords

MoS_2, dichalcogenides, sputtering, sulfurization, Raman spectrosopy.

Received: 25 May 2020
Revised: 16 July 2020
Accepted: 17 July 2020

References

1. Choudhary, N.; Park, J.; Hwang, J. Y.; Choi, W.; *ACS Appl Mater Interfaces*, **2014**, *6*, 21215.
2. Pandey, J. Soni, A.; *Applied Surface Science*, **2019**, *463*, 52.
3. Li, H.; Zhang, Q.; Yap, C. C. R.; Tay, B. K.; Edwin, T. H. T.; Olivier, A.; Baillargeat, D.; *Advanced Functional Materials*, **2012**, *22*, 1385.
4. Wang, Q. H.; Kalantar-Zadeh, K.; Kis, A.; Coleman, J. N.; Strano, M. S.; *Nat Nanotechnol*, **2012**, *7*, 699.
5. Chhowalla, M.; Shin, H. S.; Eda, G.; Li, L. J.; Loh, K. P.; Zhang, H.; *Nat. Chem.*, **2013**, *5*, 263.
6. Gusakova, J.; Wang, X. L.; Shiau, L. L.; Krivosheeva, A.; Shaposhnikov, V.; Borisenko, V.; Gusakov, V.; Tay B. K.; *Physica Status Solidi a-Applications and Materials Science*, **2017**, *214*, 1700218.
7. Mak, K. F.; Shan, J.; *Nature Photonics*, **2016**, *10*, 216.
8. Li, H.; Li, Y.; Aljarb, A.; Shi, Y.; Li, L. J.; *Chem Rev*, **2018**, *118*, 6134.
9. Cho, B.; Hahm, M. G.; Choi, M.; Yoon, J.; Kim, A. R.; Lee, Y. J.; Park, S. G.; Kwon, J. D.; Kim, C. S.; Song, M.; Jeong, Y.; Nam, K. S.; Lee, S.; Yoo, T. J.; Kang, C. G.; Lee, B. H.; Ko, H. C.; Ajayan, P. M.; Kim, D. H.; *Sci. Rep*, **2015**, *5*, 8052.
10. Park, J.; Mun, J.; Shin, J. S.; Kang, S. W.; *R. Soc. Open Sci.*, **2018**, *5*, 181462.
11. Donarelli, M.; Ottaviano, L.; *Sensors (Basel)*, **2018**, *18*.
12. Liu, B.; Chen, L.; Liu, G.; Abbas, A. N.; Fathi, M.; Zhou, C.; *ACS Nano*, **2014**, *8*, 5304.
13. Shokri, A.; Salami, N.; *Sensors and Actuators B: Chemical*, **2016**, *236*, 378.
14. Zhao, S. J.; Xue, J. M.; Kang, W.; *Chemical Physics Letters*, **2014**, *595*, 35.
15. Perkins, F. K.; Friedman, A. L.; Cobas, E.; Campbell, P. M.; Jernigan, G. G.; Jonker, B. T.; *Nano Lett.*, **2013**, *13*, 668.
16. Guo, J.; Wen, R.; Zhai, J.; Wang, Z. L.; *Science Bulletin*, **2019**, *64*, 128.
17. Barzegar, M.; Berahman, M.; Iraji Zad A.; *Beilstein J. Nanotechnol*, **2018**, *9*, 608.
18. Schleicher, M.; Fyta, M.; *ACS Applied Electronic Materials*, **2019**, *2*, 74.
19. Neri, G.; *Chemosensors*, **2017**, *5*, 21.
20. Li, H.; Wu, J.; Yin, Z.; Zhang H.; *ACC Chem Res*, **2014**, *47*, 1067.
21. Su, C. Y.; Lu, A. Y.; Xu, Y.; Chen, F. R.; Khlobystov, A. N.; Li, L. J.; *ACS Nano*, **2011**, *5*, 2332.
22. Jawaid, A.; Nepal, D.; Park, K.; Jespersen, M.; Qualley, A.; Mirau, P.; Drummy, L. F.; Vaia R. A.; *Chemistry of Materials*, **2015**, *28*, 337.
23. Nguyen, E. P.; Carey, B. J.; Daeneke, T.; Ou, J. Z.; Latham, K.; Zhuiykov, S.; Kalantar-zadeh, K.; *Chemistry of Materials*, **2014**, *27*, 53.
24. Castellanos-Gomez, A.; Barkelid, M.; Goossens, A. M.; Calado, V. E.; van der Zant, H. S.; Steele G. A.; *Nano Lett.*, **2012**, *12*, 3187.
25. Liu, Y.; Nan, H.; Wu, X.; Pan, W.; Wang, W.; Bai, J.; Zhao, W.; Sun, L.; Wang, X.; Ni Z.; *ACS Nano*, **2013**, *7*, 4202.
26. Lunceford, C.; Borcean, E.; Drucker, J.; *Crystal Growth & Design*, **2016**, *16*, 988.
27. Yang, S. Y.; Shim, G. W.; Seo, S.-B.; Choi S.-Y.; *Nano Research*, **2016**, *10*, 255.
28. Muratore, C.; Hu, J. J.; Wang, B.; Haque, M. A.; Bultman, J. E.; Jespersen, M. L.; Shamberger, P. J.; McConney, M. E.; Naguy, R. D.; Voevodin A. A.; *Applied Physics Letters*, **2014**, *104*, 261604.
29. Ohashi, T.; Suda, K.; Ishihara, S.; Sawamoto, N.; Yamaguchi, S.; Matsuura, K.; Kakushima, K.; Sugii, N.; Nishiyama, A.; Kataoka, Y.; Natori, K.; Tsutsui, K.; Iwai, H.; Ogura, A.; Wakabayashi H.; *Japanese Journal of Applied Physics*, **2015**, *54*, 04DN08.
30. Kaindl, R.; Bayer, B. C.; Resel, R.; Muller, T.; Skakalova, V.; Habler, G.; Abart, R.; Cherevan, A. S.; Eder, D.; Blatter, M.; Fischer, F.; Meyer, J. C.; Polyushkin, D. K.; Waldhauser W.; *Beilstein J. Nanotechnol*, **2017**, *8*, 1115.
31. Browning, R.; Padigi, P.; Solanki, R.; Tweet, D. J.; Schuele, P.; Evans, D.; *Materials Research Express*, **2015**, *2*, 035006.
32. Tan, L. K.; Liu, B.; Teng, J. H.; Guo, S.; Low, H. Y.; Tan, H. R.; Chong, C. Y.; Yang, R. B.; Loh K. P.; *Nanoscale*, **2014**, *6*, 10584.

33. Ishihara, S.; Hibino, Y.; Sawamoto, N.; Suda, K.; Ohashi, T.; Matsuura, K.; Machida, H.; Ishikawa, M.; Sudoh, H.; Wakabayashi, H.; Ogura A.; *Japanese Journal of Applied Physics*, **2016**, *55*, 06GF01.
34. Shahzad, R.; Kim, T.; Kang S.-W.; *Thin Solid Films*, **2017**, *641*, 79.
35. Zhong, W.; Deng, S.; Wang, K.; Li, G.; Li, G.; Chen, R.; Kwok, H. S.; *Nanomaterials (Basel)*, **2018**, *8*.
36. Huang, J.-H.; Chen, H.-H.; Liu, P.-S.; Lu, L.-S.; Wu, C.-T.; Chou, C.-T.; Lee, Y.-J.; Li, L.-J.; Chang, W.-H.; Hou T.-H.; *Materials Research Express*, **2016**, *3*, 065007.
37. Samassekou, H.; Alkabsh, A.; Wasala, M.; Eaton, M.; Walber, A.; Walker, A.; Pitkänen, O.; Kordas, K.; Talapatra, S.; Jayasekera, T.; Mazumdar, D.; *2D Materials*, **2017**, *4*, 021002.
38. Hussain, S.; Shehzad, M. A.; Vikraman, D.; Khan, M. F.; Singh, J.; Choi, D. C.; Seo, Y.; Eom, J.; Lee, W. G.; Jung J.; *Nanoscale*, **2016**, *8*, 4340.
39. Gatensby, R.; McEvoy, N.; Lee, K.; Hallam, T.; Berner, N. C.; Rezvani, E.; Winters, S.; O'Brien, M.; Duesberg G. S.; *Applied Surface Science*, **2014**, *297*, 139.
40. Pacley, S.; Hu, J.; Jespersen, M.; Hilton, A.; Waite, A.; Brausch, J.; Beck-Millerton, E.; Voevodin A. A.; *Journal of Vacuum Science & Technology A: Vacuum, Surfaces and Films*, **2016**, *34*, 041505.
41. Goel, N.; Kumar, R.; Jain, S. K.; Rajamani, S.; Roul, B.; Gupta, G.; Kumar, M.; Krupanidhi, S. B.; *Nanotechnology*, **2019**, *30*, 314001.
42. Jo, S. S.; Li, Y.; Singh, A.; Kumar, A.; Frisone, S.; LeBeau, J. M.; Jaramillo R.; *Journal of Vacuum Science & Technology A*, **2020**, *38*, 013405.
43. Matsuura, K.; Ohashi, T.; Muneta, I.; Ishihara, S.; Kakushima, K.; Tsutsui, K.; Ogura, A.; Wakabayashi, H.; *Journal of Electronic Materials*, **2018**, *47*, 3497.
44. Zhou, D.; Shu, H.; Hu, C.; Jiang, L.; Liang, P.; Chen X.; *Crystal Growth & Design*, **2018**, *18*, 1012.
45. Artyukhov, V. I.; Hu, Z.; Zhang, Z.; Yakobson, B. I.; *Nano Letters*, **2016**, *16*, 3696.
46. Zheng, W.; Qiu, Y.; Feng, W.; Chen, J.; Yang, H.; Wu, S.; Jia, D.; Zhou, Y.; Hu, P.; *Nanotechnology*, **2017**, *28*, 395601.
47. Wang, J.; Cai, X.; Shi, R.; Wu, Z.; Wang, W.; Long, G.; Tang, Y.; Cai, N.; Ouyang, W.; Geng, P.; Chandrashekar, B. N.; Amini, A.; Wang, N.; Cheng, C.; *ACS Nano*, **2018**, *12*, 635.
48. Eda, G.; Yamaguchi, H.; Voiry, D.; Fujita, T.; Chen, M.; Chhowalla M.; *Nano Lett*, **2011**, *11*, 5111.